# Influence of slicing parameters on surface quality and mechanical properties of 3D-printed CF/PLA composites fabricated by FDM technique

N. Vinoth Babu [a], N. Venkateshwaran [a, *], N. Rajini [b, *], Sikiru Oluwarotimi Ismail [c], Faruq Mohammad [d], Hamad A. Al-Lohedan [d] and Suchart Siengchin [e]

[a] Department of Mechanical Engineering, Rajalakshmi Engineering College, Thandalam, Chennai, Tamil Nadu, India.

[b] Centre for Composite Materials, Department of Mechanical Engineering, Kalasalingam Academy of Research and Education, Krishnankoil 626126, Tamil Nadu, India.

[c] Centre for Engineering Research, Department of Engineering, School of Physics, Engineering and Computer Science, University of Hertfordshire, Hatfield, AL10 9AB, England, United Kingdom.

[d] Department of Chemistry, College of Science, King Saud University, P.O. Box 2455, Riyadh, Kingdom of Saudi Arabia 11451.

[e] Department of Materials and Production Engineering, The Sirindhorn International Thai-German Graduate School of Engineering (TGGS), King Mongkut's University of Technology North Bangkok, Bangkok, Thailand.

*Corresponding authors: N. Rajini, rajiniklu@gmail.com, Tel.: +91 9942139392

N. Venkateshwaran, venkateshwaran.n@rajalakshmi.edu.in

## Abstract

The carbon fiber reinforced polymer matrix composites play an important role in many applications, due to their high strengths and moduli. Hence, this present study focuses on evaluation of mechanical properties of three dimensional (3D)-printed carbon fiber/polylactic acid (CF/PLA) composites, using fused deposition modeling (FDM) technique. The composites were prepared with different slicing parameters: layer heights or thicknesses (0.08, 0.25 and 0.64 mm), infill densities (20, 40, 60 and 80%) and layer patterns (rectilinear, triangular and hexagonal). The 3D-printed CF/PLA composite samples were subjected to tensile, flexural and interlaminar shear strength

(ILSS) tests to assess the influence of the aforementioned process parameters on their mechanical characteristics. Further investigations were carried out to evaluate the effect of surface roughness of the samples on their mechanical properties. From the test results obtained, it was evident that both rectilinear and hexagonal patterns exhibited better mechanical properties at infill density and layer thickness of 60% and 0.64 mm, respectively. The fractured samples were examined, using scanning electron microscopy (SEM). The images depicted that lesser layer thickness produced poor CF/PLA interfacial bonding/adhesion and major failure mode was traced to fiber pull-out. Therefore, engineering application of the various 3D-printed CF/PLA composite samples evidently depends on their slicing parameters, as studied.

**Keywords:** CF/PLA composite, AM/3D-printing, FDM, Mechanical properties, SEM.

## 1. Introduction

With advent of Industry 4.0, new digital industrial revolution, additive manufacturing (AM) or three dimensional (3D) printing plays a major role in manufacturing engineering. It is the next phase in digitization of the manufacturing sector [1]. AM is also a challenging process, because of the trial and error method that is used to identify the combination of factors: material, printer, process parameters, post-processing in a quest to obtain a desired output of the end product [2]. AM enables quicker manufacturing of physical models directly from 3D computer-aided design (CAD) data without any conventional tooling or huge programming requirements. It also offers greater flexibility in design, which allows creation and visualization of design ideas into successful prototypes and final products [3].

AM is one of the major components of Industry 4.0, due to the necessity of mass customization, lesser prototype construction, fewer dies, less post processing, among other benefits. Various 3D printing technologies include, but are not limited to, fused deposition modelling (FDM), selective laser sintering (SLS), stereo-lithography (SL), photopolymerization (PPT), laminated object manufacturing (LOM) and solid ground curing (SGC). A wide variety of polymeric materials are available for AM process, based on their applications. Commonly used liquid polymeric materials are epoxy resin, acrylic resin and binder/powder hybrids. Powdered form of polymers include polyamides (PA12 and PA11), polycarbonate (PC), polystyrene (PS), acryl butadiene

styrene (ABS), ABS–PC blend, polypropylene (PP), polyphenyl sulfone (PPSU), starch, elastomer/cellulose, polylactic acid (PLA), thermoplastic polyurethane (TPU), poly ether ether ketone (PEEK), high-density polyethylene (HDPE), polyethylenimine (PEI). Solid sheet polymeric materials widely used are polyester film, polyolefin and poly vinyl copolymer films as well as thermosetting and thermoplastic films.

Due to growing concern for environmental pollution and reduction in the availability of petroleum-based plastics, researchers have focused on the filaments from bioplastics, in particular PLA for various structural and biomedical applications. In order to increase the strength of the PLA, reinforcements are also being used. The PLA is environmentally friendly material, when compared with petroleum-based ABS, polyethylene and polypropylene [4]. The structure of PLA is harder than that of ABS and has melting temperature in the range of 180-220 °C, which is lower than that of ABS [5]. The filament-based technology, FDM with wide variety of material in the form of filament is being frequently used across various sectors, especially for functional parts [6-9].

Moreover, various studies have been carried out with respect to FDM technology. To start with, Chacon et al. [10] investigated into the effect of build orientation, layer thickness and mechanical performance of PLA samples, using FDM technology. It was observed that on-edge orientation provided better strength, stiffness and ductility. The results obtained by Gianluca et. al. [11] showed that unmodified polymer filaments were not good choice for FDM process, by correlating the rheology and thermo-mechanical properties. Leipeng [12] studied the optimization of some parameters, such as nozzle diameter, liquefier temperature, extrusion velocity, filling velocity and layer thickness. They were varied to achieve higher tensile strength and lower surface roughness with less build time on FDM PLA printed parts. Yash et al. [13] investigated into the influence of various parameters: infill densities of 50, 75 and 100%, layer thicknesses of 0.1, 0.2 and 0.3 mm as well as shell thicknesses of 0.6, 0.8 and 1.0 mm of PLA material through FDM. The results showed that the mechanical properties increased with an increase in layer thickness. The influence of printing temperature, printing speed, layer thickness and filling ratio on mechanical properties of PLA filament was carried out by Boddula et al. [14] and recorded optimal printing speed of 60 mm/s, layer thickness of 0.25 mm, printing temperature of 210 °C and filling rate of 60%. Jose et al. [15] studied the mechanical properties of 3D- printed composites, using PLA–graphene filament with honey comb infill pattern, flat build orientations and

different infill percentages of 22, 78, 10 and 50% and layer heights of 0.13, 0.27 and 0.20 mm. The results showed that tensile strength was significantly influenced by infill and layer thickness. The carbon fiber reinforced with polyethylene terephthalate glycol (PETG) composites by Halil et al. [16] depicted that addition of fibers reduced the voids in 3D-printed samples, whereas the orientation of fibers was better in molded samples.

In addition, Fuda et al. [17] investigated into the carbon fiber reinforced with ABS to fabricated various composites, using FDM by varying the reinforcement weight percentages: 3, 5, 7.5, 10 and 15. It was observed that 5 wt.% of carbon fiber content had a better tensile strength and 7.5 wt.% counterpart recorded a higher tensile modulus. Comparative study carried out by Ryosuke et al. [18] on carbon fiber/PLA and jute fiber/PLA composite showed that the addition of carbon fiber tremendously increased their mechanical properties, when compared with neat PLA. The study on various process parameters: infill densities of 20, 40 and 60%, extrusion temperatures of 200 and 220 °C, raster angles of 0°/90° and 45°/+45° and layer thicknesses of 0.1 and 0.2 mm of PLA has been carried out by Joao Fernandes [19]. The results showed that a better tensile strength was achieved with an infill of 60%, extrusion temperature of 220 °C, raster angle of 0°/90° and layer thickness of 0.1 mm. Miguel et al. [20] investigated into the effect of graphene and nano-platelet added PLA on the mechanical properties of corresponding composites with three different orientations: flat edge, on-edge and upright. The results depicted that flat edge and on-edge orientations showed better mechanical properties, when compared with upright orientation.

Moving forward, Vigneshwaran et al. [21] carried out statistical analysis of mechanical properties of biodegradable wood/PLA composites. Various layer heights of 0.08, 0.16 and 0.24 mm, infill of 30, 60 and 90% and patterns of layer: triangle and hexagon were studied. It was reported that better properties were achieved with an increase in both infill percentage and layer pattern. The effect of different patterns on the energy absorption capability of the tubes made of PLA and carbon fiber reinforced PLA composite has been investigated by Quanjin et al. [22]. The results revealed that the triangular and square patterns showed negative effect on the energy absorption.

Besides, surface finish quality of AM is becoming more and more vital with more printed parts being used by end-users. It is critical not only for better functionality and appearance of the end products, but also for cost reduction regarding reduced post-processing of 3D-printed parts and overall prototyping time reduction. The dimensional

accuracy of the parts produced with FDM 400MC machine was less accurate in producing a circular shaped parts, as reported by Sudin et al. [23]. Additional studies on dimensional accuracy and surface quality of 3D-printed structure, using FDM technology are subsequently elucidated.

Bakar et al. [24] investigated into the dimensional accuracy and surface quality of multiple features with various process parameters of FDM. Dyrbus [25] studied the dimensional accuracy by FDM process and obtained dimensional accuracies of 0.1 mm and 0.4°. With the help of design of experiments, Galantucci et al. [26] analyzed the dimensional accuracy on rectangular test samples, minimizing changes in length, width and height for both industrial 3D printing system and an open-source type. Habeeb et al. [27] studied the tensile strength and porosity of open-source fused filament fabrication (FFF) machine and observed that it was comparable with the parts manufactured by mid-range commercial machine. One of the main problems in the AM parts included obtaining good surface quality and this was greatly affected, due to complex geometries [28], chordal error attributed to tessellation and slicing [29], layered deposition of material [30], layer height and wall thickness [31] as well as print orientation angle [32].

From the afore-reported studies, it was observed that the poor surface finish quality in final products of the FDM process has been attributed to the layer-upon-layer deposition and improper process parameters, such as an infill pattern. Furthermore, the end product quality depends on the following parameters: layer thickness, infill density and pattern, air gaps, build orientation, flow rate, fiber orientation, extrusion temperature, deposition speed, number of shells/perimeter, fiber volume fraction as well as raster angle and width. To ensure better surface integrity, the manufacturing process parameters must be carefully selected. Also, the effect of printing parameters on the surface roughness and wettability of 3D-printed materials must be investigated, especially with reference to layer thickness. Therefore, this present work investigated into the effect of process parameters, such as infill pattern, infill percentage and layer thickness on mechanical properties and surface roughness of 3D-printed carbon fiber/poly lactic acid (CF/PLA) composites. The fractured surfaces of the samples were examined to obtain various relevant SEM images required to describe the failure modes associated with the 3D-printed CF/PLA composite samples and establish possible reasons.

## 2. Materials and methods

### *2.1. Materials*

The material utilized was PLA reinforced with carbon fiber. It was purchased from NANOVIA Smart Chemicals Advance Materials, France. The properties of the PLA filament are presented in Table 1.

**Table 1**

Properties of CF/PLA filament used.

| Property | Value |
|---|---|
| Density | 1.3 g/cm$^3$ (1300 kg/m$^3$) |
| Melting temperature | 190 – 230 °C |
| Heat deflection | 21 to 85 °C |

### *2.2. FFF of composite*

Fig. 1 shows the schematic of FFF process, where filaments on the spools were fed into the liquefier head through a driven gear and grooved bearing, and extruded above the glass transition temperature. The first layer was deposited over the print bed, which moved downward of one desired layer thickness. The process was repeated in the same manner till the part was completed. Using Raise 3D V2 N2 Hot end 3D printer, the tensile, flexural and interlaminar shear strength (ILSS) samples were printed, using CF/PLA composite filament. Before printing, the model was checked to have stereolithography (STL) file format and avoid errors during printing. Generally, CAD application produce error in STL files include gaps, normal faces, self-convergence, noise shells and manifold errors.

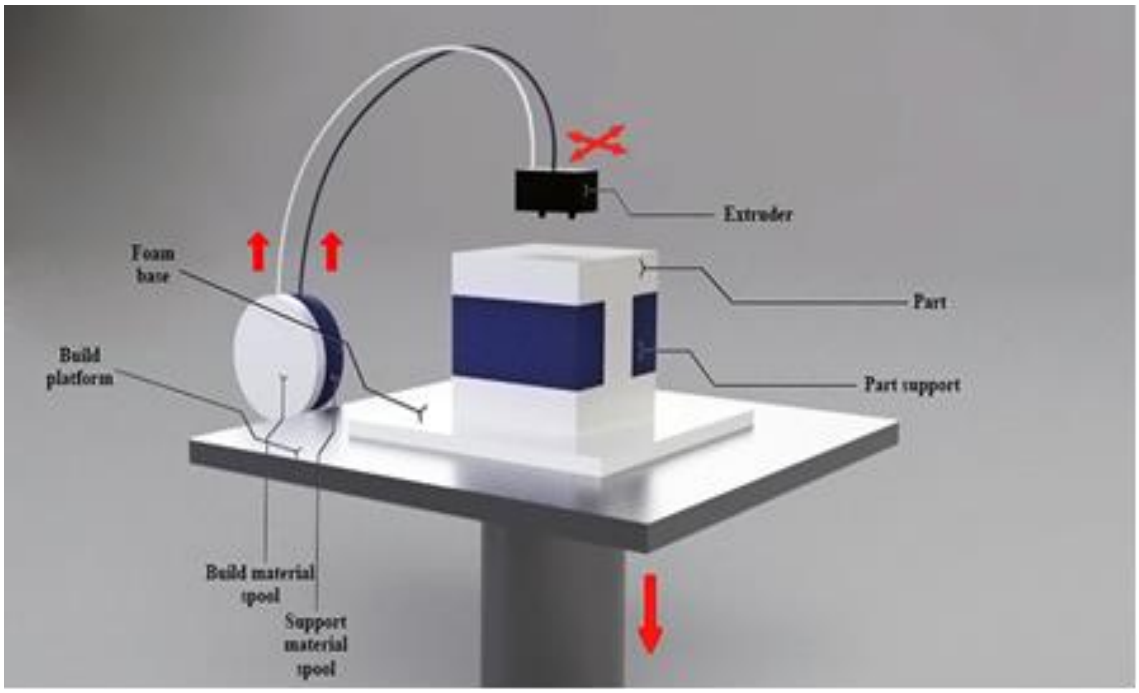


**Fig. 1.** Schematic view of FDM process.

Additionally, the problems in the model can be corrected during first stage of the STL generation process, known as *fix*. The STL file opens in a dedicated slicer and this slider chops up STL file into numerous horizontal layers, based on the machine setting and process parameter conditions. All these data are bundled up into a G Code file and it was uploaded into the 3D printer. Then, this printer separated two dimensional (2D) layers to reassemble a 3D object on the print bed by successive deposition of layer upon layer. The sequential steps used during fabrication of all the 3D-printed composite samples are shown in Fig. 2. The machine process parameters are presented in Table 2.

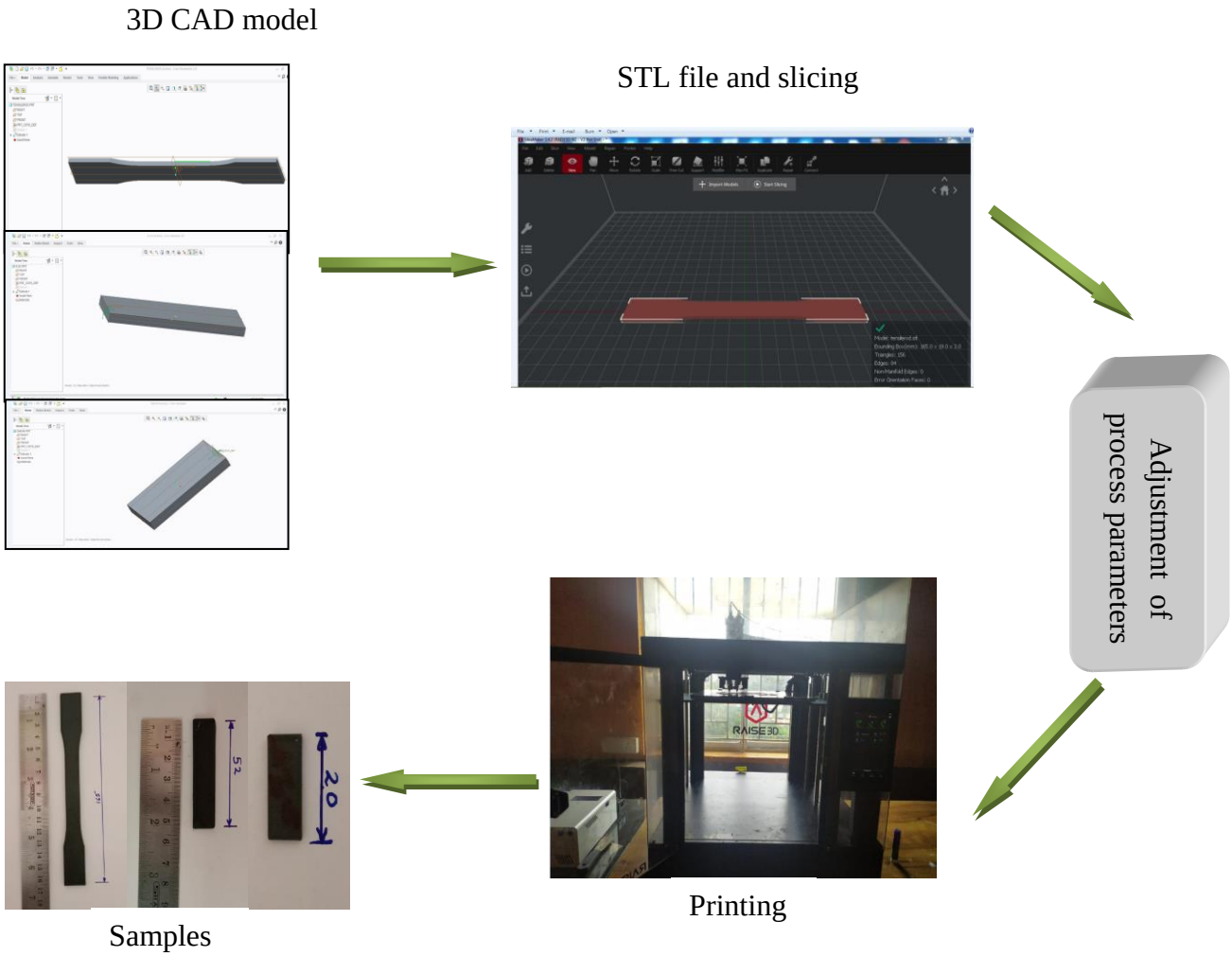


**Fig. 2.** Sequential steps used during fabrication of the 3D-printed composite samples, using FDM.

**Table 2**

FDM machine process parameters.

| Parameters | Units | Values |
|---|---|---|
| Nozzle diameter | Mm | 0.4 |
| Nozzle temperature | °C | 240 |
| Print bed temperature | °C | 90 |
| Contours | Shell | 02 |

The geometries of all the prepared samples for this work are tabulated in Table 3, they were used to conduct the various mechanical tests. In the matrix Table, the samples with rectilinear pattern are designated as $R_1$, $R_2$, $R_3$,…, $R_{12}$ for various infill percentages (%) and different layer thicknesses (mm). Similarly, samples with triangular and hexagonal patterns are designated as $T_1$, $T_2$, $T_3$,…, $T_{12}$ and $H_1$ , $H_2$, $H_3$,…, $H_{12}$,

respectively for various infill percentages (%) and different layer thicknesses (mm). Fig. 3 shows the different test samples and various in fill patterns used in this work.

**Table 3**

Matrix data for the 3D-printed composite samples, showing their combined process parameters.

| Layer height / thickness (mm) | Infill density ( % ) | Types of pattern and their designations | | |
|---|---|---|---|---|
| | | Rectilinear | Triangular | Hexagonal |
| 0.08 | 20 | $R_1$ | $T_1$ | $H_1$ |
| | 40 | $R_2$ | $T_2$ | $H_2$ |
| | 60 | $R_3$ | $T_3$ | $H_3$ |
| | 80 | $R_4$ | $T_4$ | $H_4$ |
| 0.25 | 20 | $R_5$ | $T_5$ | $H_5$ |
| | 40 | $R_6$ | $T_6$ | $H_6$ |
| | 60 | $R_7$ | $T_7$ | $H_7$ |
| | 80 | $R_8$ | $T_8$ | $H_8$ |
| 0.64 | 20 | $R_9$ | $T_9$ | $H_9$ |
| | 40 | $R_{10}$ | $T_{10}$ | $H_{10}$ |
| | 60 | $R_{11}$ | $T_{11}$ | $H_{11}$ |
| | 80 | $R_{12}$ | $T_{12}$ | $H_{12}$ |

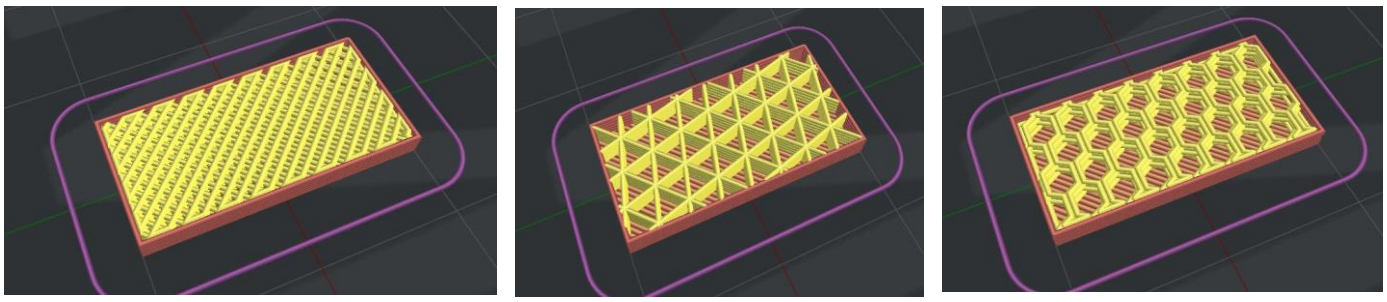

(a) (b) (c)

**Fig. 3.** Selected infill patterns: (a) rectilinear, (b) triangular and (c) hexagonal.

*2.3. Testing methods*

The tensile, flexural and ILSS properties of the samples, prepared using FFF process were evaluated in accordance with the American society for testing and materials (ASTM) standards; D638, D790 and D2344. The prepared samples and experimental set-ups for tensile, flexural and ILSS tests are shown in Figs 4, 5 and 6, respectively.

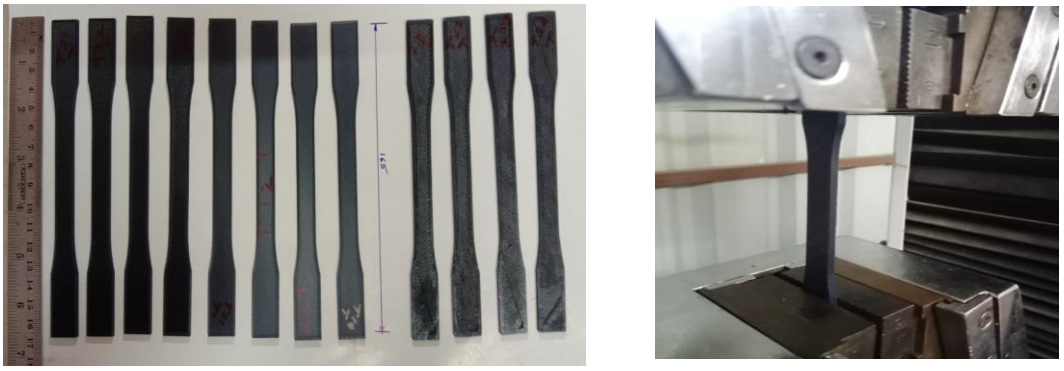

(a) (**b)**

**Fig. 4.** (a) 3D-printed tensile test samples and (b) tensile test set-up.

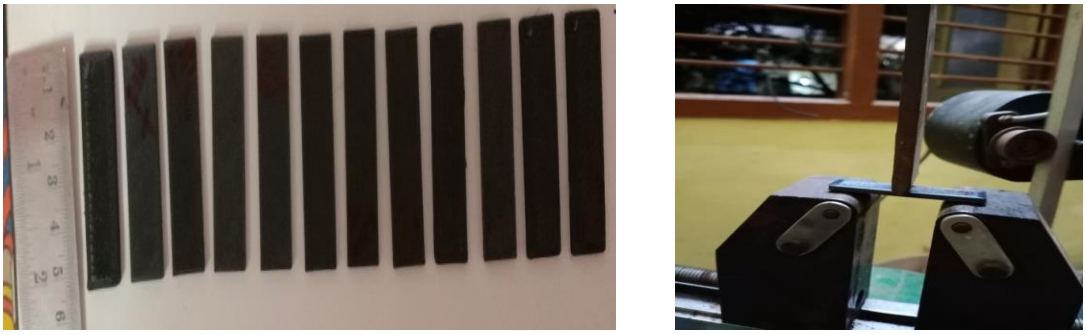

**(a) (b)**

**Fig. 5.** (a) 3D-printed flexural test samples and (b) three-point bending/flexural test set-up**.**

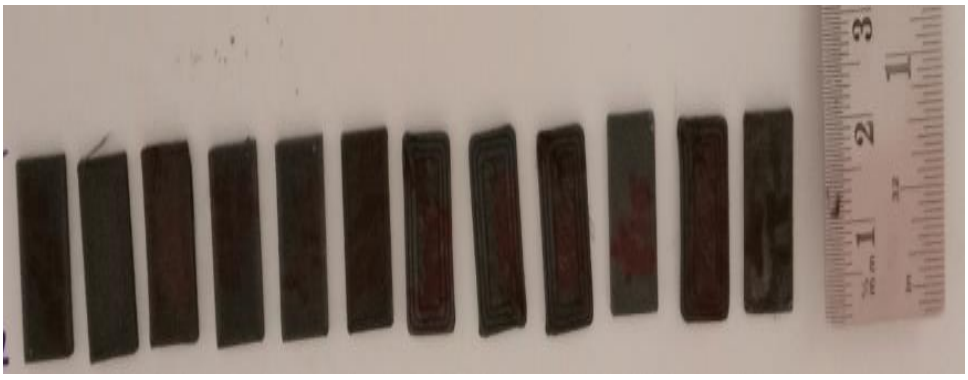

**Fig. 6.** 3D-printed ILSS test samples.

*2.4. Surface roughness testing*

One of the main problems associated with the additive manufactured parts is the surface roughness, when compared with conventional counterparts. Surface roughness plays a major role in engineering applications. Therefore, the effects of printing parameters, such as layer pattern, layer thickness and infill density on the surface roughness of the samples were investigated (Fig. 7).

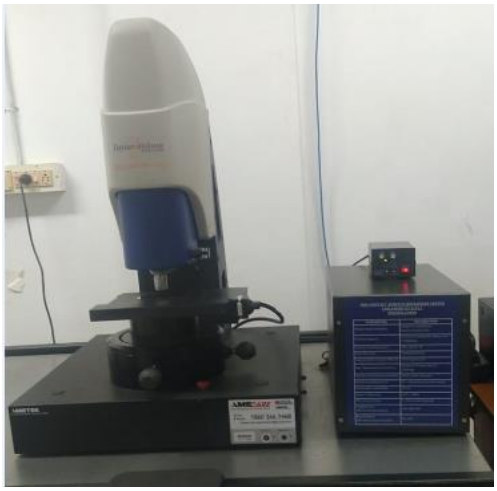

**Fig. 7.** Surface roughness measurement set-up.

Measurements of how surface component deviated with actual surface in the direction normal to the surface were taken. A Taylor Hobson stylus surface profilometer (Fig. 7) was used to obtain the surface roughness values, $R_a$ – arithmetic mean deviation of the roughness profile, 2D and 3D forms, contour and other parameters. The measurements and their corresponding values were recorded, as displayed on the screen and tabulated.

## 3. Results and discussion

The tensile, flexural and shear properties of all the 3D-printed samples with selected combination of infill density, layer thickness and layer pattern were determined, evaluated according to the ASTM standards and subsequently elucidated.

*3.1. Tensile properties of CF/PLA composites*

From the experimentation, the stress-strain plots for the various samples were obtained. Therefore, the stress-strain plots for rectilinear, triangular and honeycomb or

hexagonal patterns are shown in Figs 8(a), (b) and (c), respectively. The tensile properties namely, tensile strengths and moduli of the samples are presented graphically, as depicted in Figs 9 and 10 for different layer patterns.

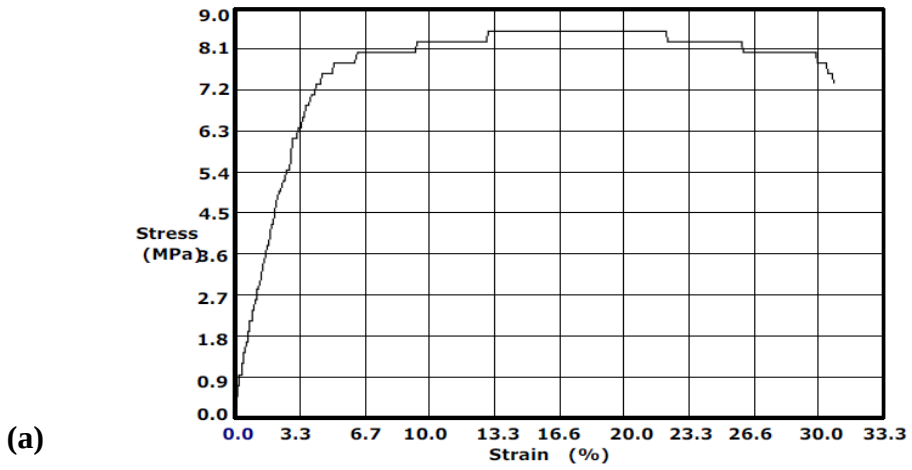


**(a)**

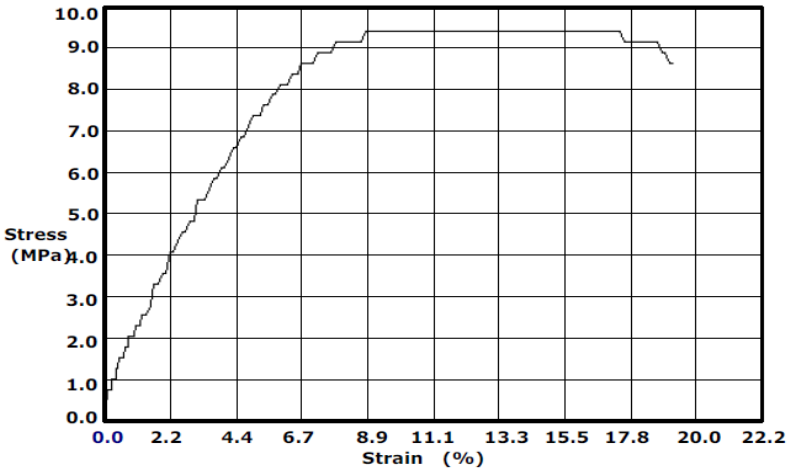


**(b)**

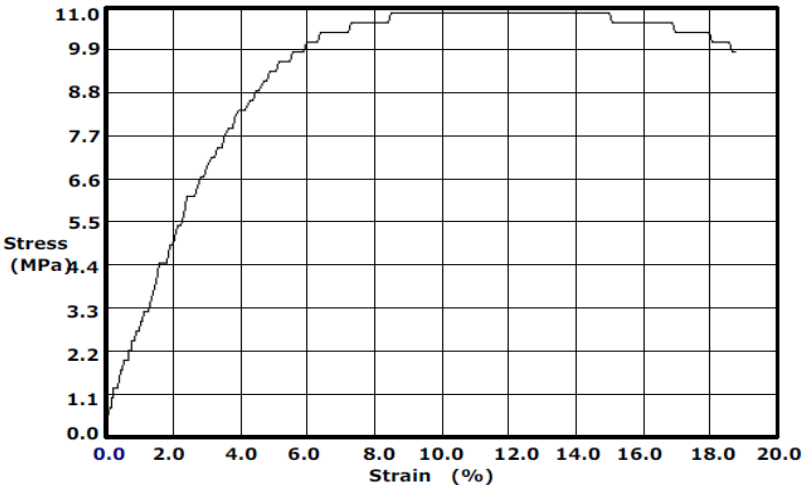


**(c)**

**Fig. 8.** Stress-strain plots for (a) rectilinear, (b) triangular and (c) hexagonal patterns, with layer height of 0.25 mm and infill density of 20%.

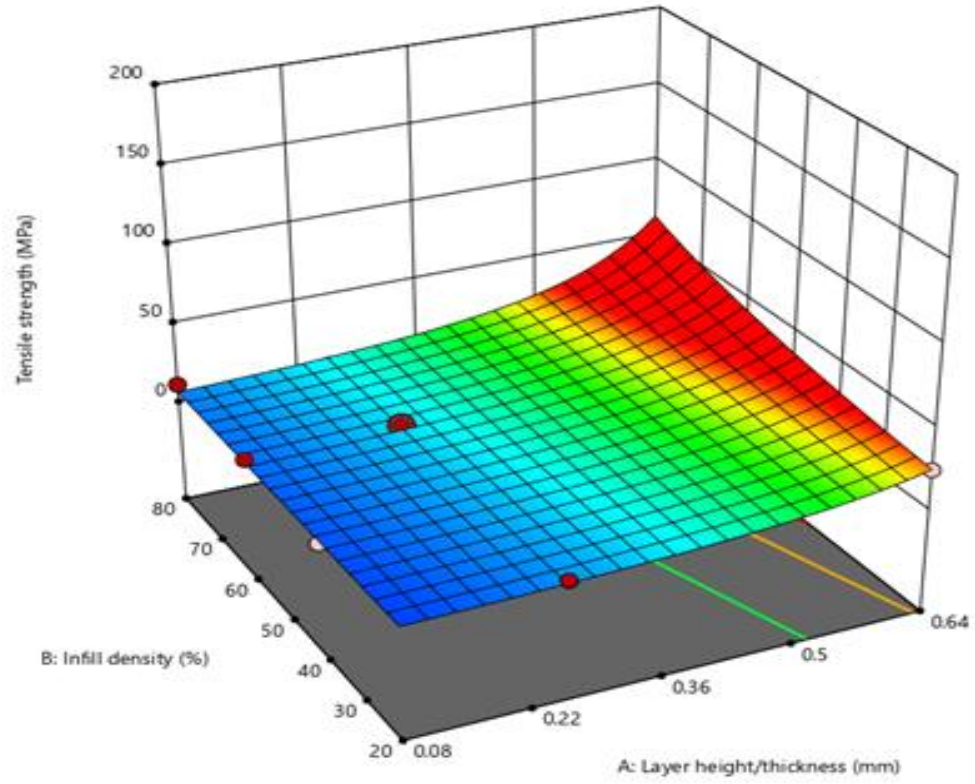


(a) Rectilinear pattern.

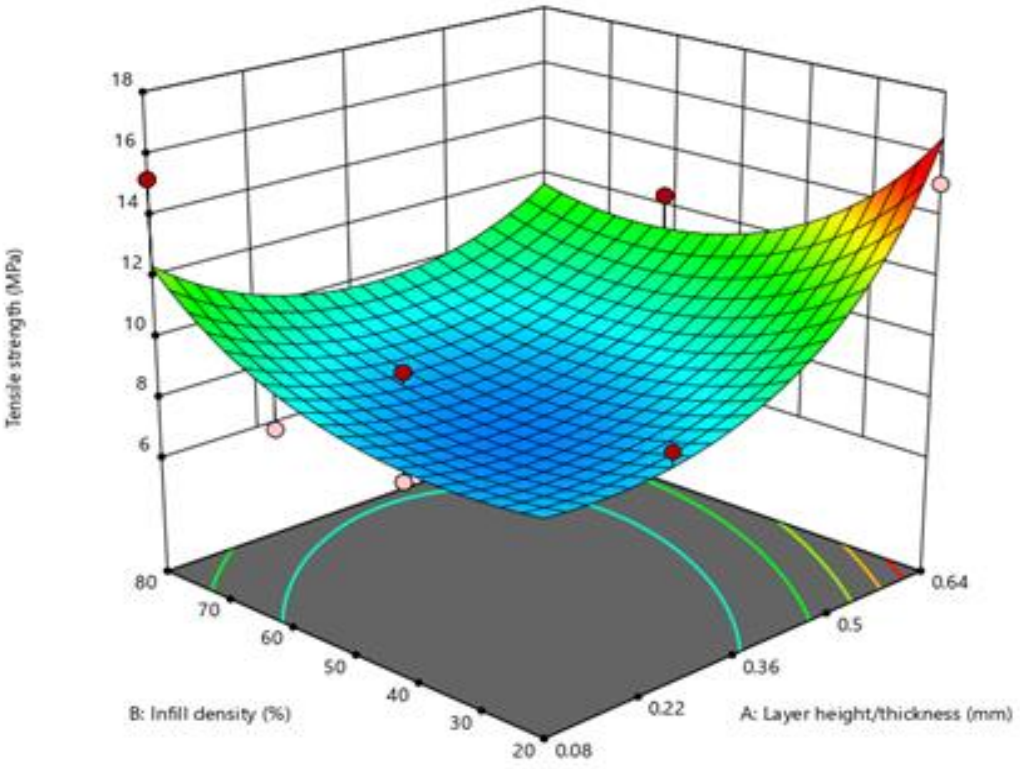


(b) Triangular pattern.

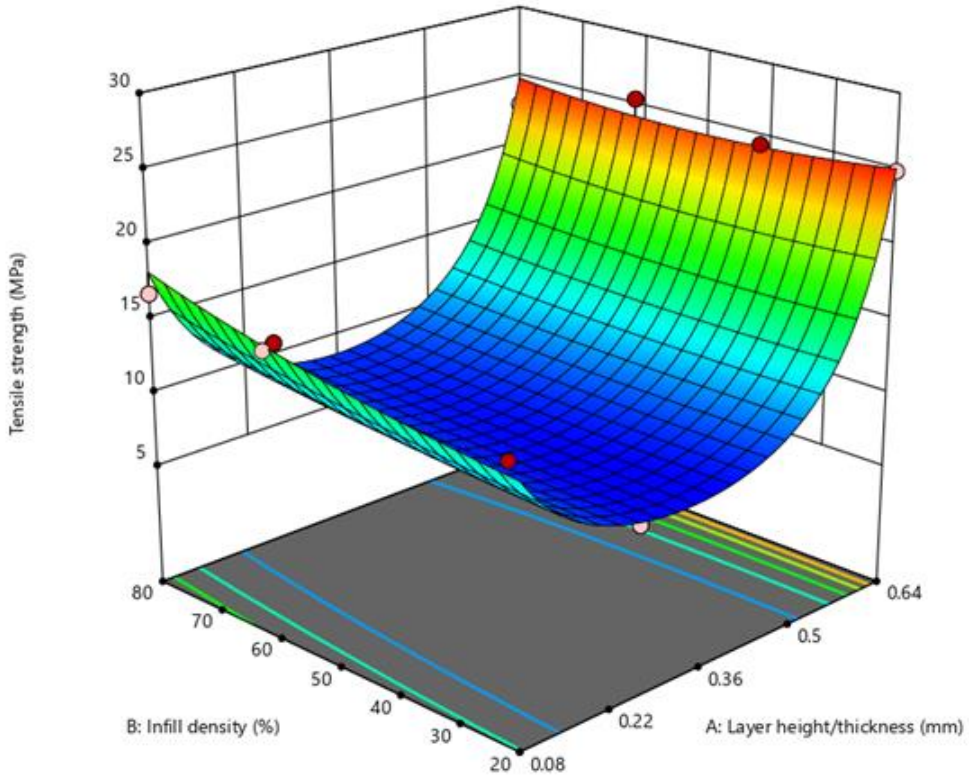


(c) Hexagonal pattern

**Fig. 9.** Tensile strengths of the various patterned 3D-printed composite samples.

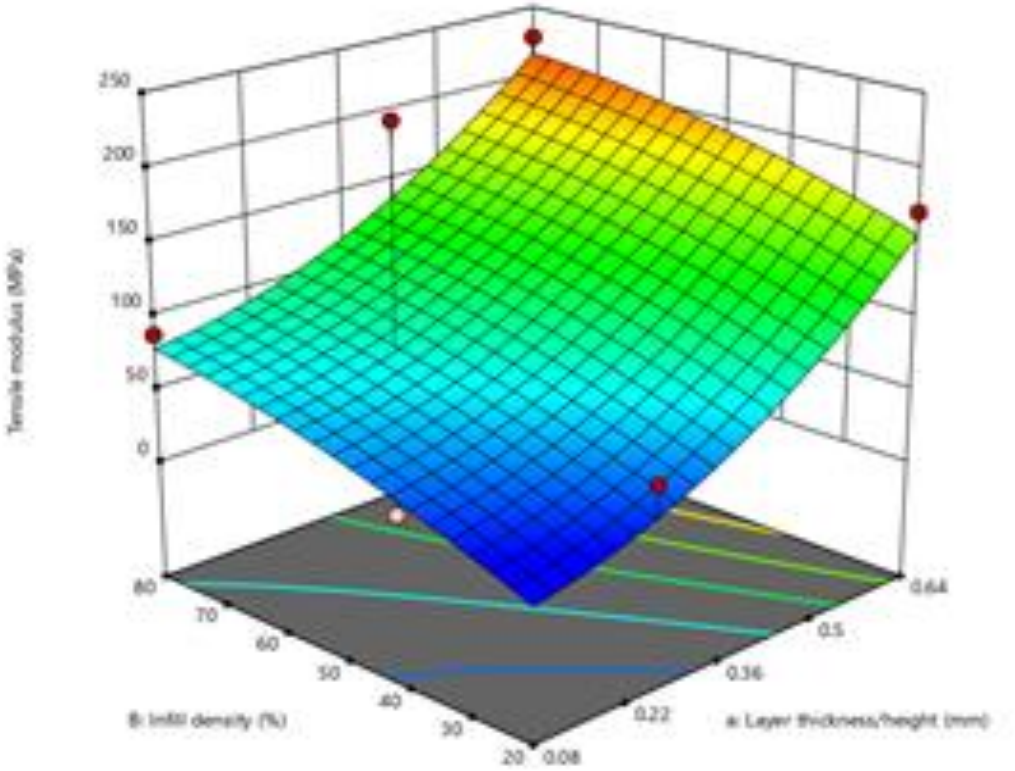


(a) Rectilinear pattern.

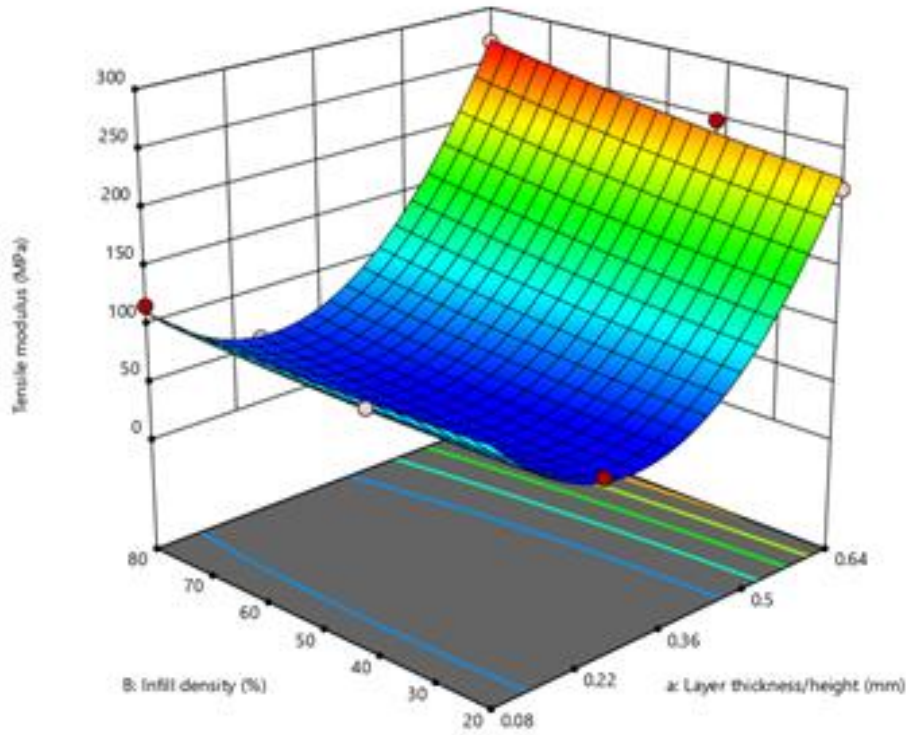


(b) Triangular pattern.

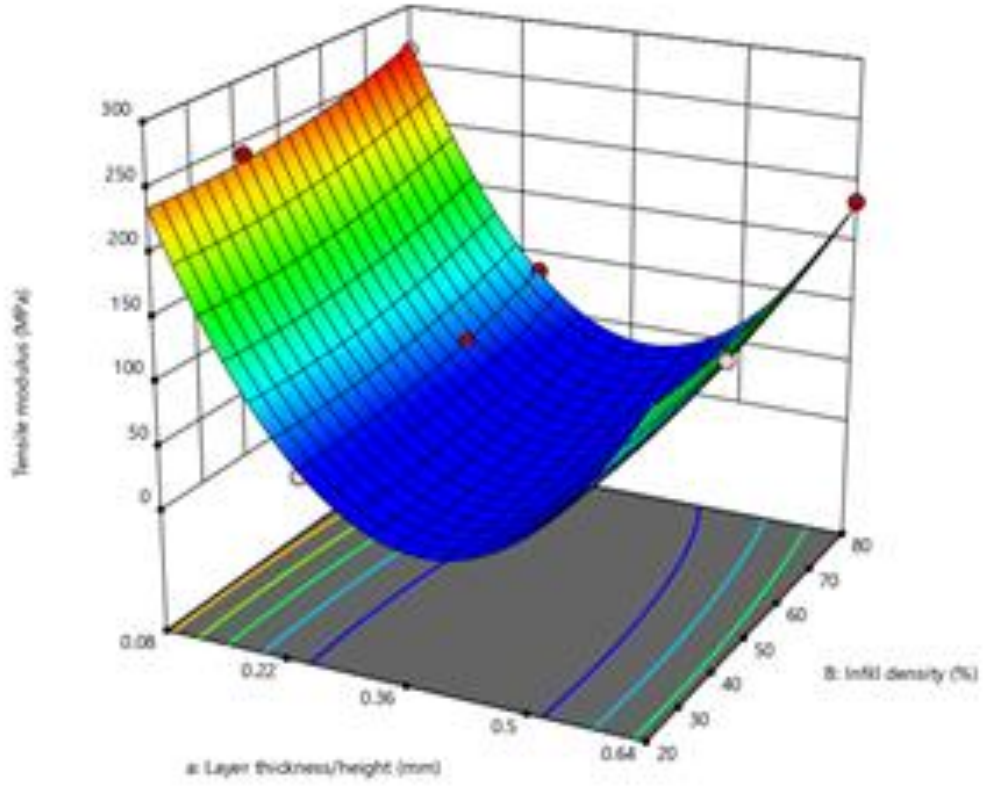


(c) Hexagonal pattern.

**Fig. 10.** Tensile moduli of the various patterned 3D-printed composite samples.

Moving forward, from the stress-strain plots, it was observed that the adhesion between PLA and carbon fibers were quite good. However, the fibers detached after it reached a maximum load. This further showed that the added fibers carried the load till it was pulled out from the matrix. At a lower infill percent, it can be assumed that voids were created during the printing, which became stress concentration areas and allowed initiation of cracks. This crack grew rapidly during testing and reached a critical length that resulted into sudden failure. This failure mechanism can be ascribed to the presence of porosity, cracks and local deformation [33]. In general, the tensile strength and modulus increased with an increase in the percentage of infill density, as earlier reported from similar studies [33-35].

Summarily, Table 4 presents the complete values of all the tests conducted under different combinations of the parameters used.

**Table 4**

Consolidated values of tensile strengths and moduli, flexural strengths and moduli as well as ILSS for the various combinations of parameters.

| Sample | Layer pattern | Layer height / thickness (mm) | Infill density (%) | Tensile strength (MPa) | Tensile modulus (MPa) | Flexural strength (MPa) | Flexural modulus (GPa) | Shear strength (MPa) |
|---|---|---|---|---|---|---|---|---|
| $R_1$ | Rectilinear | 0.08 | 20 | 1.18 | 18.3515 | 33.333 | 5.007 | 4.444 |
| $R_2$ | Rectilinear | 0.08 | 40 | 2.84 | 29.5833 | 33.333 | 5.007 | 4.722 |
| $R_3$ | Rectilinear | 0.08 | 60 | 7.34 | 68.4063 | 30.000 | 2.003 | 4.722 |
| $R_4$ | Rectilinear | 0.08 | 80 | 11.13 | 87.9842 | 36.667 | 5.007 | 5.000 |
| $R_5$ | Rectilinear | 0.25 | 20 | 8.05 | 52.1036 | 36.667 | 3.004 | 4.444 |
| $R_6$ | Rectilinear | 0.25 | 40 | 4.97 | 21.7031 | 36.667 | 5.007 | 5.000 |
| $R_7$ | Rectilinear | 0.25 | 60 | 8.52 | 27.6893 | 40.000 | 4.507 | 5.278 |
| **$R_8$** | **Rectilinear** | **0.25** | **80** | **4.97** | **19.4902** | **40.000** | **2.927** | **5.556** |
| $R_9$ | Rectilinear | 0.64 | 20 | 24.62 | 171.2100 | 40.000 | 1.502 | 5.000 |
| $R_{10}$ | Rectilinear | 0.64 | 40 | 22.96 | 157.8007 | 36.667 | 3.338 | 4.722 |
| $R_{11}$ | Rectilinear | 0.64 | 60 | 23.20 | 233.6354 | 43.333 | 5.341 | 6.111 |
| $R_{12}$ | Rectilinear | 0.64 | 80 | 28.41 | 228.1928 | 43.333 | 4.507 | 5.270 |
| $T_1$ | Triangular | 0.08 | 20 | 11.41 | 104.9678 | 40.000 | 3.338 | 3.500 |
| $T_2$ | Triangular | 0.08 | 40 | 8.32 | 241.1594 | 36.667 | 2.504 | 4.250 |

| | | | | | | | | |
|---|---|---|---|---|---|---|---|---|
| $T_3$ | Triangular | 0.08 | 60 | 8.45 | 229.6196 | 36.667 | 2.504 | 4.500 |
| $T_4$ | Triangular | 0.08 | 80 | 15.22 | 262.4138 | 36.667 | 4.507 | 4.250 |
| $T_5$ | Triangular | 0.25 | 20 | 9.41 | 48.9594 | 36.667 | 6.510 | 4.000 |
| $T_6$ | Triangular | 0.25 | 40 | 7.25 | 40.7303 | 30.000 | 6.677 | 4.500 |
| $T_7$ | Triangular | 0.25 | 60 | 9.00 | 65.5499 | 43.333 | 5.007 | 4.750 |
| $T_8$ | Triangular | 0.25 | 80 | 8.11 | 85.6389 | 43.333 | 2.504 | 5.000 |
| $T_9$ | Triangular | 0.64 | 20 | 15.07 | 161.1765 | 40.000 | 2.604 | 5.000 |
| $T_{10}$ | Triangular | 0.64 | 40 | 12.08 | 138.8506 | 33.333 | 2.671 | 3.750 |
| $T_{11}$ | Triangular | 0.64 | 60 | 12.40 | 129.1667 | 46.667 | 5.759 | 4.250 |
| $T_{12}$ | Triangular | 0.64 | 80 | 11.21 | 184.3750 | 43.333 | 6.343 | 4.000 |
| $H_1$ | Hexagonal | 0.08 | 20 | 15.55 | 168.4724 | 56.667 | 2.504 | 3.750 |
| $H_2$ | Hexagonal | 0.08 | 40 | 15.30 | 102.8917 | 43.333 | 2.003 | 3.750 |
| $H_3$ | Hexagonal | 0.08 | 60 | 15.79 | 122.8794 | 43.333 | 3.004 | 4.250 |
| $H_4$ | Hexagonal | 0.08 | 80 | 16.78 | 117.1788 | 56.667 | 1.602 | 4.000 |
| $H_5$ | Hexagonal | 0.25 | 20 | 7.90 | 49.5298 | 53.333 | 1.502 | 4.250 |
| $H_6$ | Hexagonal | 0.25 | 40 | 8.80 | 56.4103 | 53.333 | 2.114 | 3.500 |
| $H_7$ | Hexagonal | 0.25 | 60 | 8.39 | 49.4111 | 60.000 | 3.672 | 4.500 |
| $H_8$ | Hexagonal | 0.25 | 80 | 10.86 | 57.8275 | 60.000 | 3.255 | 4.500 |
| $H_9$ | Hexagonal | 0.64 | 20 | 24.93 | 216.7826 | 56.667 | 3.561 | 4.250 |
| $H_{10}$ | Hexagonal | 0.64 | 40 | 24.43 | 248.0203 | 60.000 | 2.754 | 3.500 |
| **$H_{11}$** | **Hexagonal** | **0.64** | **60** | **25.42** | **235.8071** | **60.000** | **4.674** | **4.250** |
| $H_{12}$ | Hexagonal | 0.64 | 80 | 22.95 | 269.0504 | 56.667 | 1.558 | 4.500 |

Also, it was observed from sample $H_{11}$ of hexagonal pattern that the combination of layer height of 0.64 mm and infill density of 60% produced better tensile strength and modulus of 28.41 MPa and 2.3581 MPa, respectively (Table 4). The result showed that high level of infill density resulted to a lesser amount of void and subsequently higher strength [18]. In addition, the results implied that both infill density and layer height were proportional to the strengths of the 3D-printed composite samples. Both layer height and infill percentage increased progressively with the tensile values. The hexagonal pattern samples showed an increased tensile strength, when compared with both rectilinear and triangular patterns. This can be attributed to their due to their honey comb structure, which is very strong, occupied large space, light in weight and not buckle easily when bent. Also, it can be observed that the bonding zone between

different layers were different on each pattern. In honey comb pattern, each layer laid down on a similar previous layer, whereas the bonding zone between each layer corresponded only with the points where the filament crossed the previous layer filaments in rectilinear pattern. These characteristics can similarly be traced to the honeycomb patterns with higher tensile moduli [19]. The stress-strain plots further showed that the hexagonal pattern exhibited a large strain to failure, because of the addition of carbon fiber and it consequently reduced the stiffness of the composite samples. Hence, the 3D-printed composite can be used for the strength application rather than stiffness.

### *3.2. Flexural properties of CF/PLA composites*

The flexural strength values were plotted as a function of layer height, infill density and patterns, as shown in Figs 11(a), (b) and (c) for rectilinear, triangular and hexagonal patterns, respectively, and similarly plots for modulus values are presented in Figs 12(a), (b) and (c) for rectilinear, triangular and hexagonal patterns, respectively.

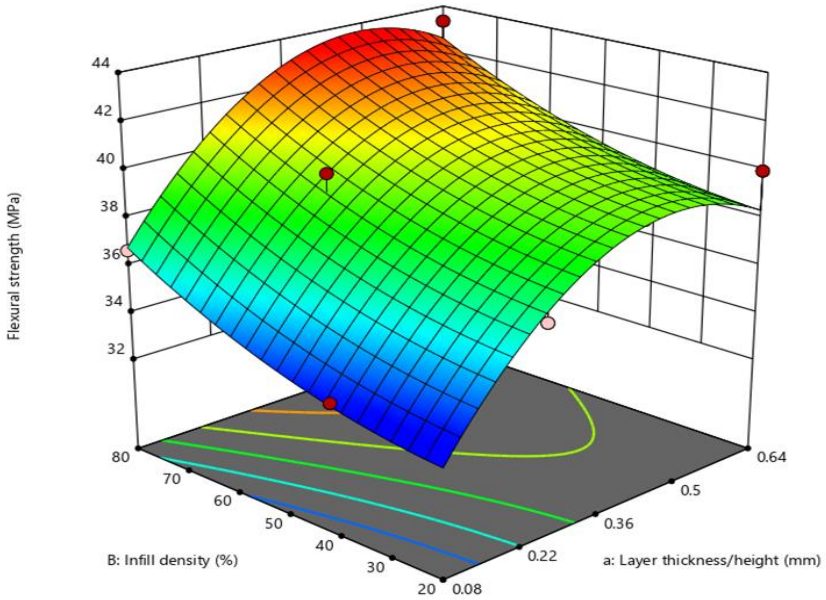


(a) Rectilinear pattern.

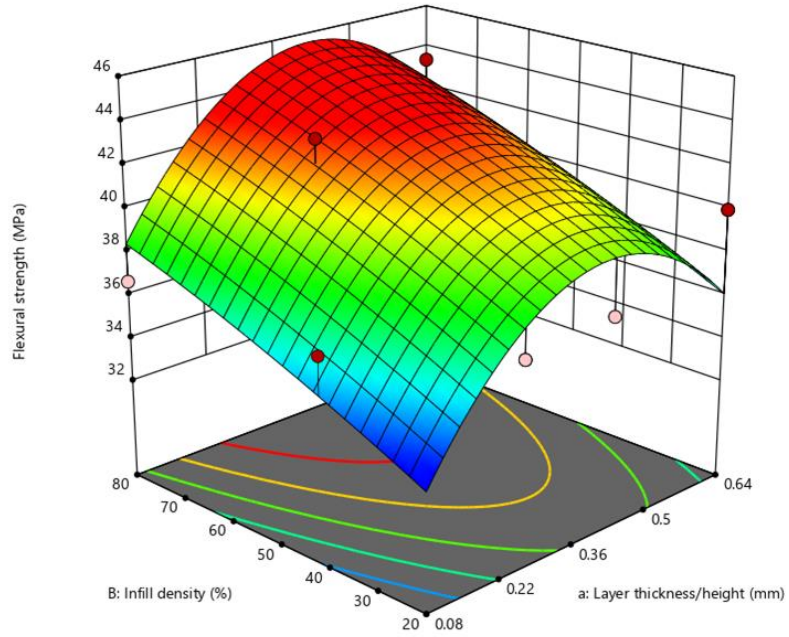


(b) Triangular pattern.

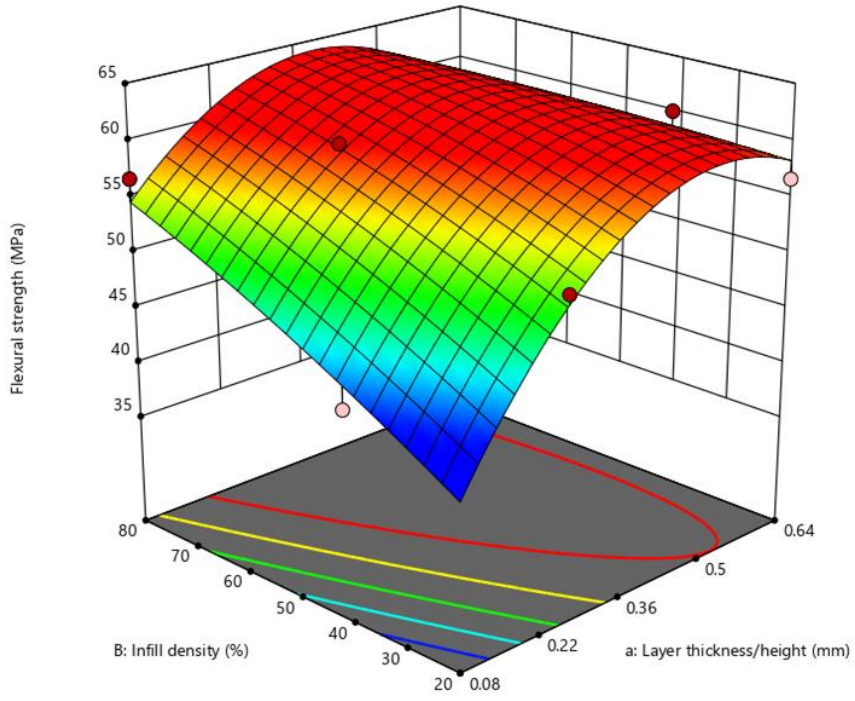


(c) Hexagonal pattern

**Fig. 11.** Flexural strengths of the various patterned composite samples.

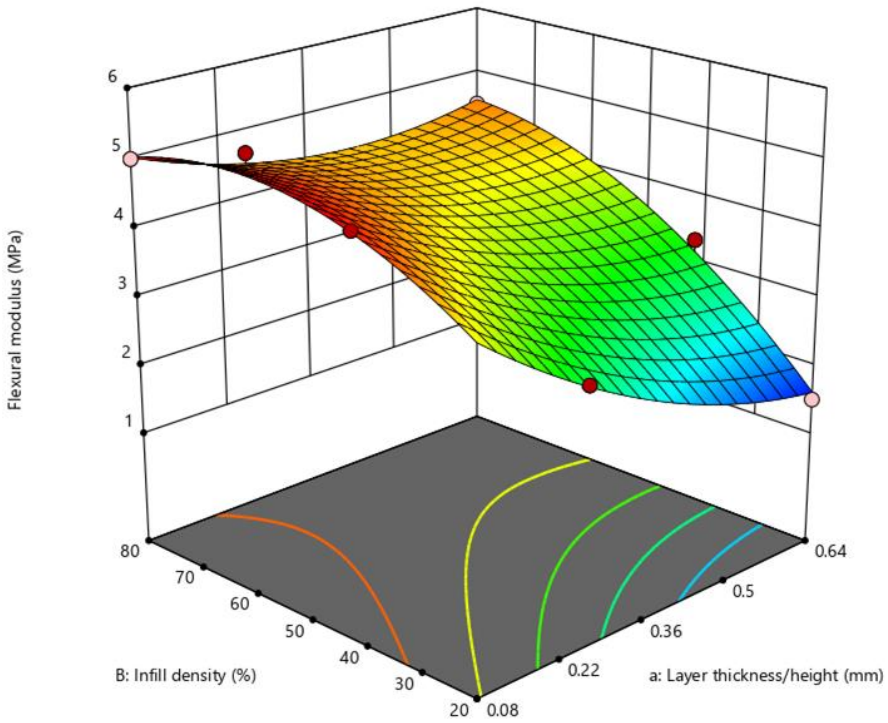


(a) Rectilinear pattern.

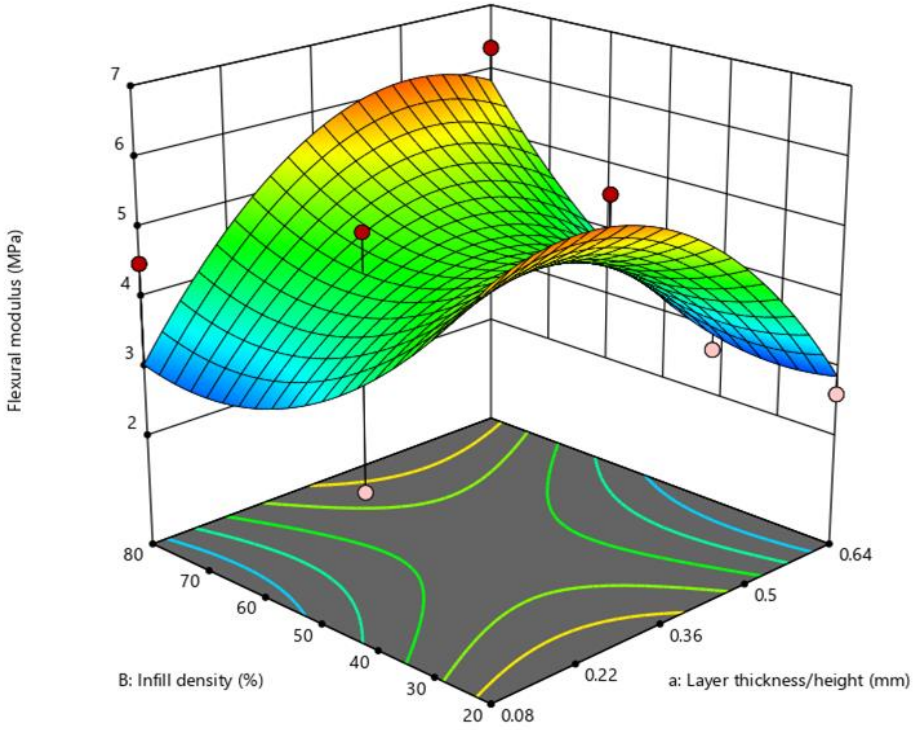


(b) Triangular pattern.

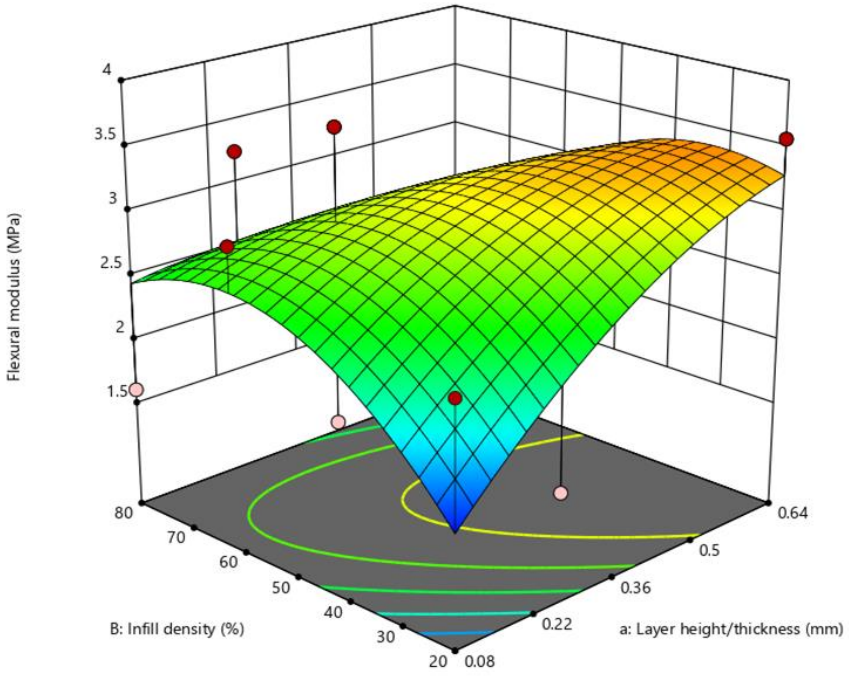


(c) Hexagonal pattern.

**Fig. 12.** Flexural moduli of the various patterned composite samples.

From the results obtained, it was evident that the samples with higher layer thickness and highest infill density recorded the highest flexural strength. For instance, rectilinear pattern of layer thickness of 0.64 mm and infill density of 60% yielded flexural strength of 60 MPa. Similarly, high flexural strength of 60 MPa was obtained from both triangular and hexagonal layer patterns with different infill densities of 60 and 80%, respectively. In general, an increase in both strength and modulus was obtained when the percentage of infill density of the sample increased. Furthermore, samples with larger layer thickness required more cooling time, which resulted to a better adhesion between the layers. Additional reason behind decrease in the strength and modulus include the direction of the geometry during deposition [35]. From this, it can be established that the layer pattern with more infill percentage provided a better bending strength.

*3.3. ILSS properties of CF/PLA composite*

The rationale behind ILSS test was to analyze the effect of presence of carbon fiber reinforcement on the bonding performance of CF/PLA composites of different layer patterns, layer thicknesses and infill densities. The ultimate shear strengths were obtained and plotted for the samples with various layer patterns, layer thicknesses and infill densities, as shown in Figs 13(a), (b) and (c) for rectilinear, triangular and hexagonal patterns, respectively.

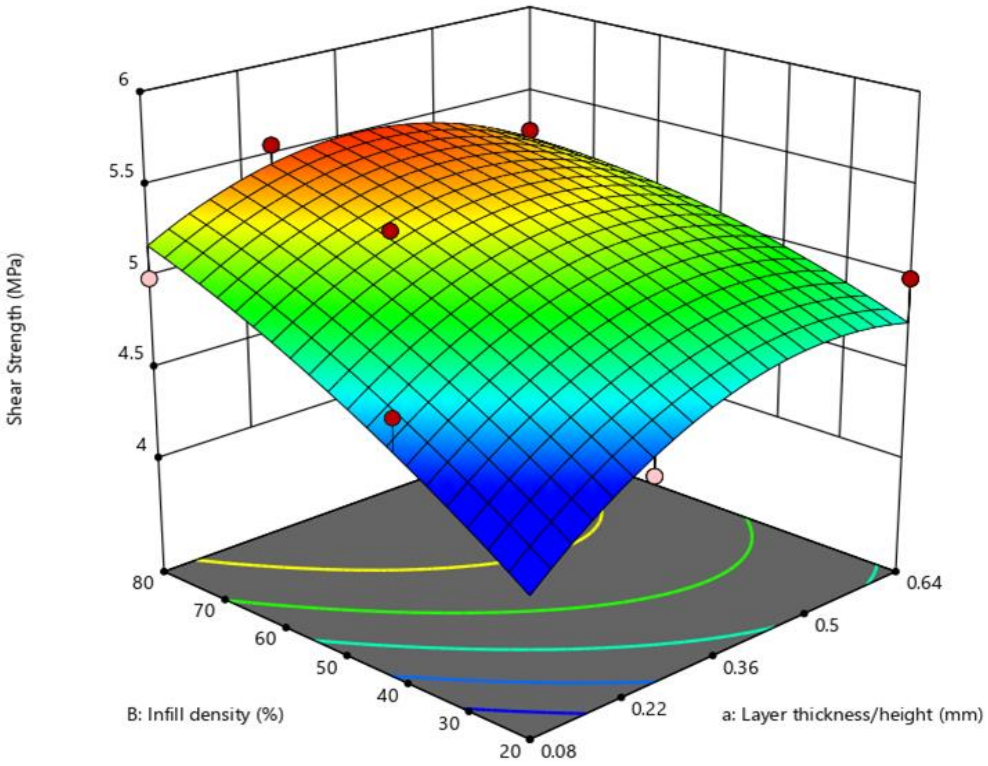


(a) Rectilinear pattern.

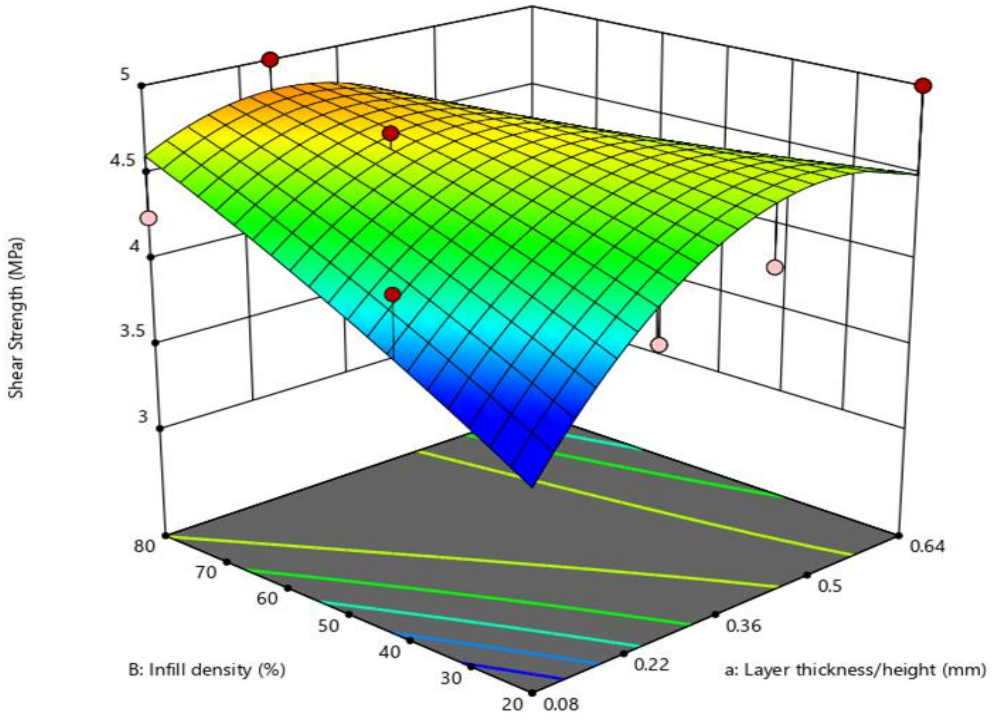


(b) Triangular pattern.

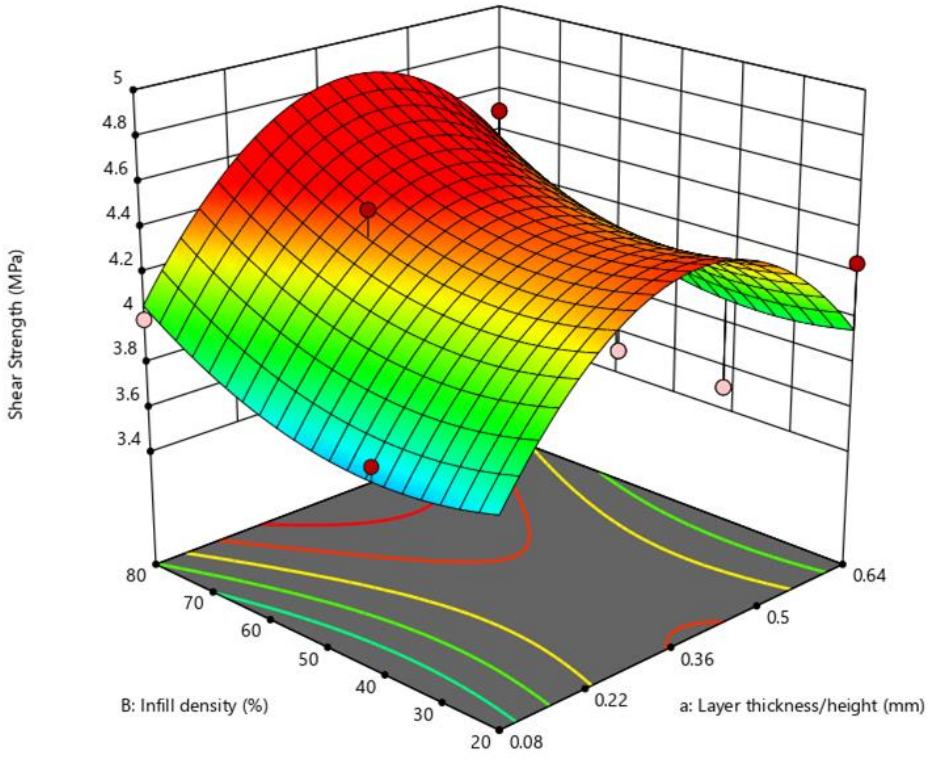


(c) Hexagonal pattern.

**Fig. 13.** Shear strengths of the various patterned composite samples.

From the plotted values, it was observed that maximum shear strength of 5.556 MPa was obtained with rectilinear pattern of 0.25 mm layer thickness and 80% infill density, as shown in Fig. 13(a). Similarly, rectilinear pattern with layer thickness of 0.25 mm as well as 60 and 80% infill densities recorded same maximum shear strength of 5.556 MPa. Then, the triangular pattern followed closely next to the rectilinear pattern with 60 and 80% infill densities, as depicted in Fig. 13(b) and previously presented in Table 4. While, samples $H_6$ and $H_{10}$ of hexagonal pattern recorded the lowest shear strength value of 3.500 MPa (Fig. 13c), similar to that of $T_1$. From these results, layer thickness and infill density mainly influenced the shear strength value. An increased infill density and layer height reduced the problem of void and interfacial adhesion and thereby provided enhanced shear strength [35]. Hence, layer thickness and/or height determined the strength of the additively manufactured/3D-printed parts. As previously discussed that an increased layer thickness resulted to better mechanical properties. Therefore, by increasing the layer thickness, the number of joints between layers was reduced, which resulted to a lesser stress concentration and consequently, a greater strength of the 3D-printed composite sample was obtained. More also, deposited material with a larger layer thickness had more cooling time, which resulted to a stronger adhesion between the layers [36].

### *3.4. SEM characterization of fractured CF/PLA composite*

Fig. 14(a) shows that an improved mechanical strength was achieved with a rectilinear pattern, due to a better interfacial adhesion between carbon fiber and PLA matrix. Fig. 14(b) depicts that the main reason for the failure can be attributed to the fiber pull-out, due to the poor adhesion at interface, as rampantly evident in triangular pattern. However, due to an increase in infill percent, a better adhesion at their interface was also observed from the SEM images. Besides, SEM image showed a large number of voids and poor interfacial adhesion between the matrix and fiber on the fractured surface area. Fig. 14(c) shows that hexagonal pattern strained in a larger manner before the ultimate failure. Hence, the reason behind better mechanical properties achieved with hexagonal pattern, especially after the fiber failure can be attributed to the capability of the PLA matrix to take up the applied load and exhibited a larger elongation before a complete failure finally occurred.

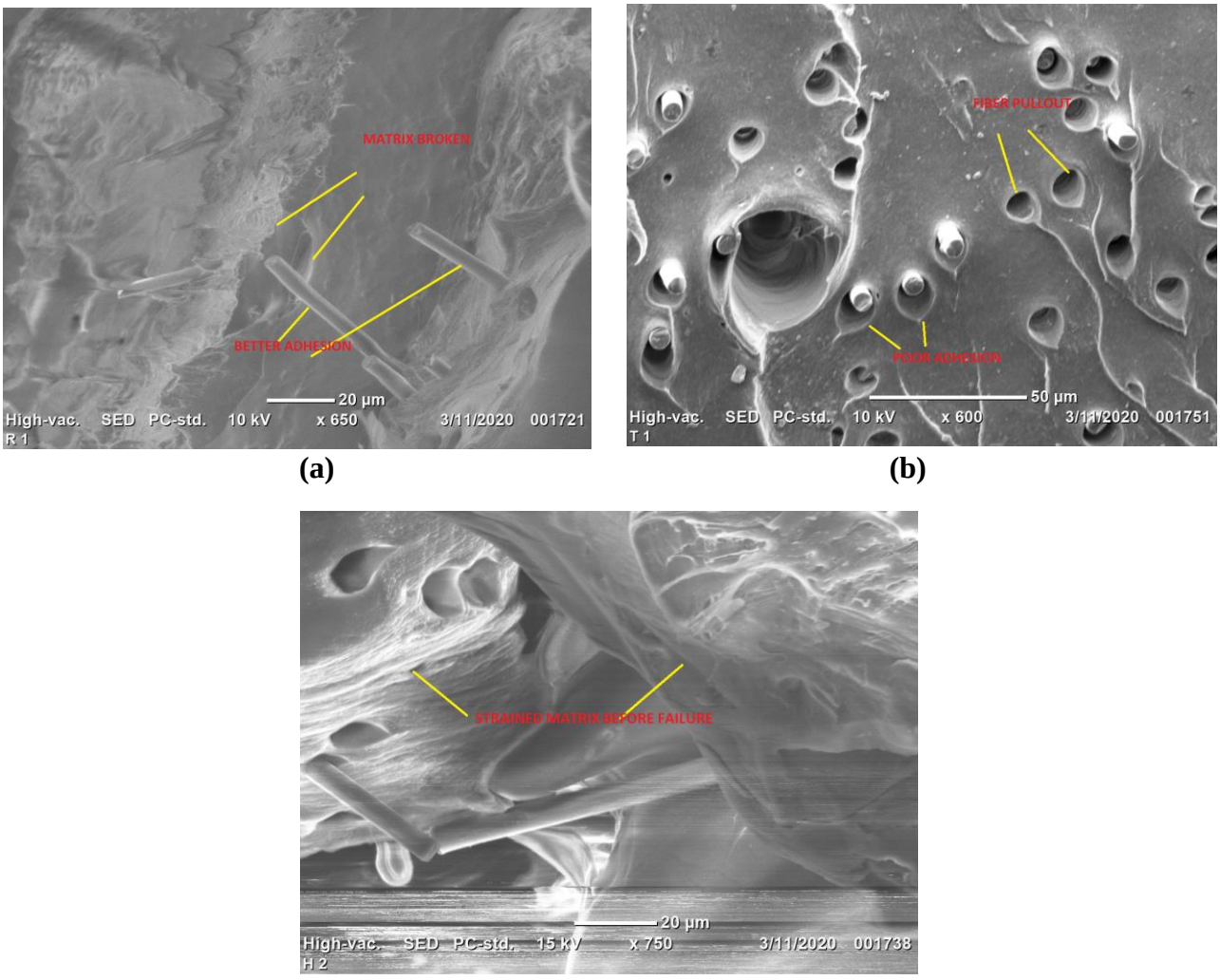


**(a)** **(b)**

(c)

**Fig. 14.** SEM images of fractured surfaces of the (a) rectilinear, (b) triangular and (c) hexagonal patterns.

*3.5. Surface roughness and its effects on properties*

The surface finish of the AM fabricated samples was unduly rough, due to layered pattern of material deposition. Because of this problem, material properties were affected significantly and hence analyses on how surface roughness affected the properties of the fabricated samples were obtained. Therefore, Figs 15, 16 and 17 show the roughness values of the surfaces of tensile, flexural and ILSS fractured 3D-printed composite samples. From Figs 15(a), (b) and (c), it was observed that the surface roughness values of the tensile samples were 28.76, 36.41 and 65.7 µm for hexagon, rectilinear and triangular patterns, respectively. Similarly, for flexural fractured

samples, the roughness values were 29.30, 35.50 and 45.90 µm for hexagon, rectilinear and triangular patterns, as shown in Figs 16(a), (b) and (c), respectively. The ILSS samples recorded surface roughness values of 42.00, 47.10 and 53.80 µm for rectilinear, hexagon and triangular patterns, as depicted in Figs 17(a), (b), and (c), respectively. This analysis evidently showed that the surface roughness directly influenced the tensile, flexural and ILSS of the 3D-printed CF/PLA composite samples. It was observed that the lower roughness values produced better mechanical properties and *vice versa.*

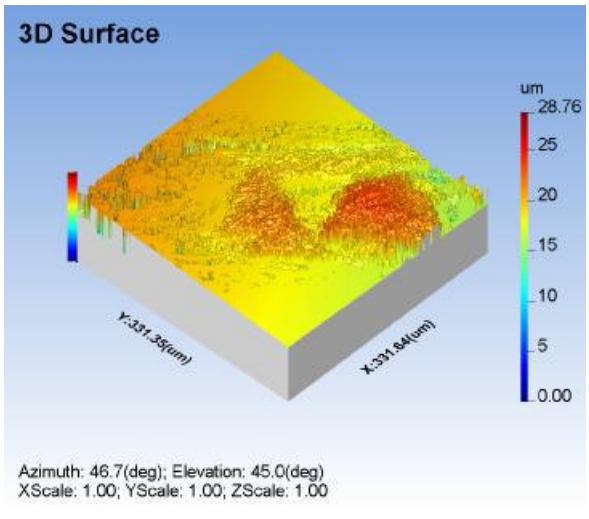


(a) Hexagonal pattern.

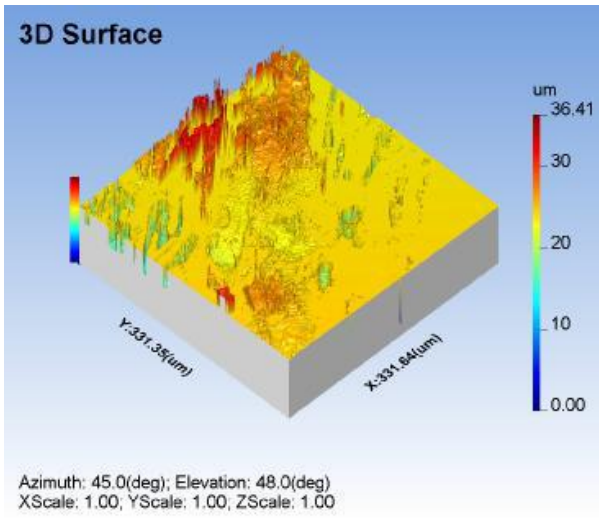


(b) Rectilinear pattern.

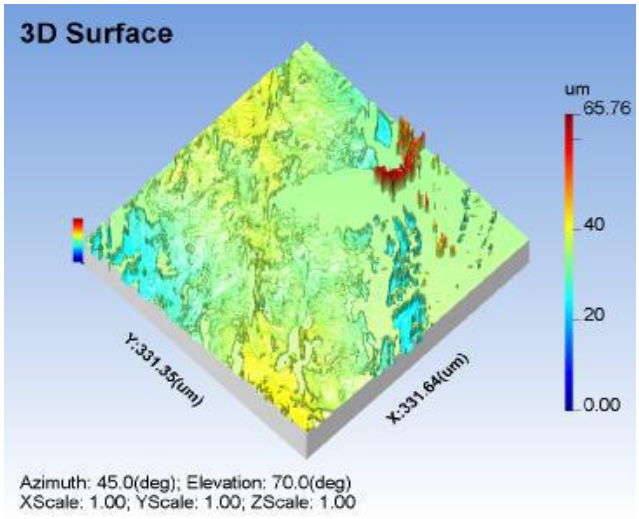


(c)Triangular pattern.

**Fig. 15.** Surface roughness of the tensile fractured surfaces of various patterned 3D-printed composite samples.

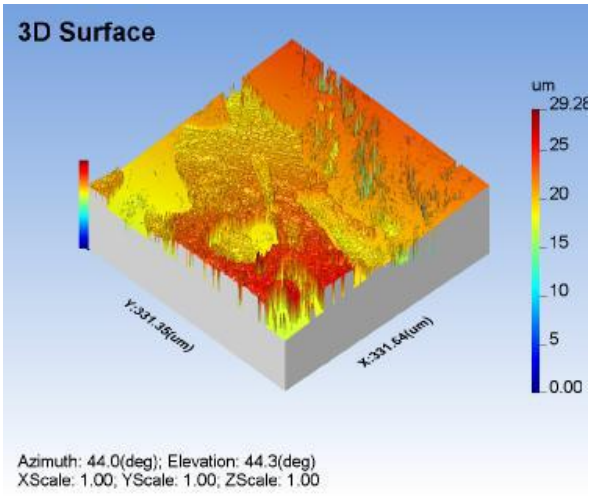


(a) Hexagonal pattern.

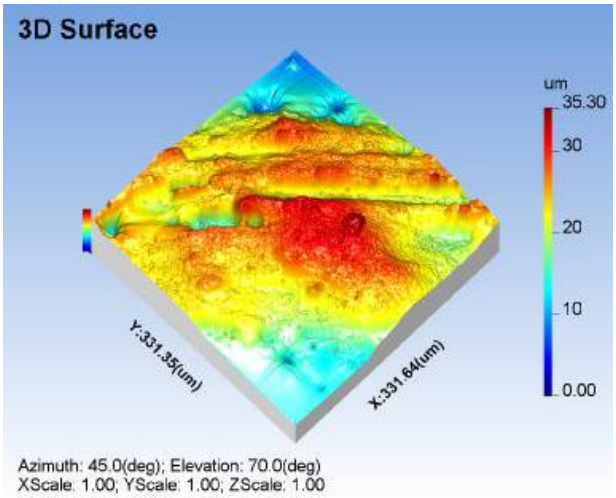


(b) Rectilinear pattern.

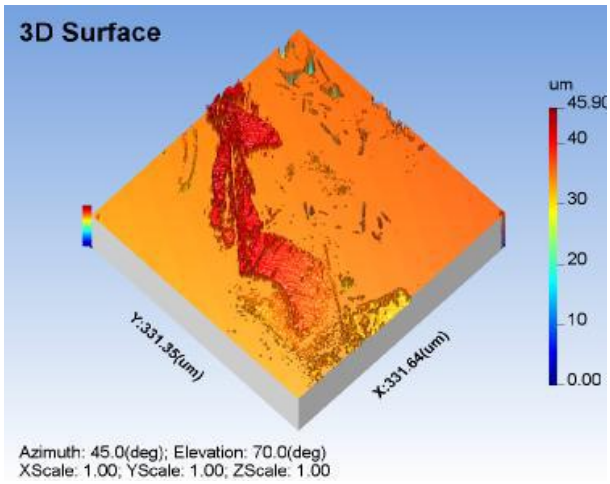


(c) Triangular pattern.

**Fig. 16.** Surface roughness of the flexural fractured surfaces of various patterned 3D-printed composite samples.

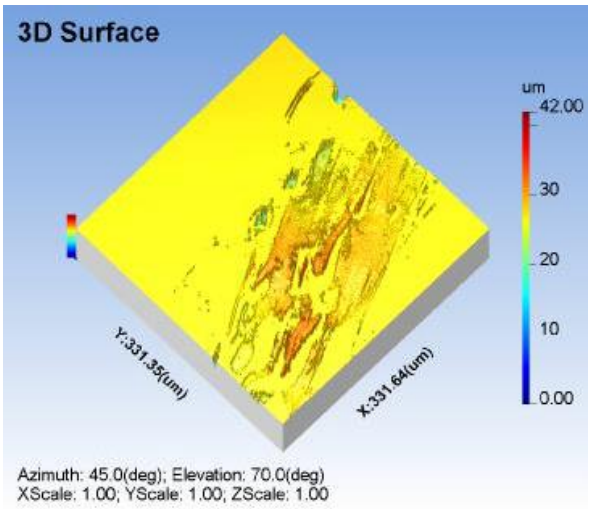


(a) Rectilinear pattern.

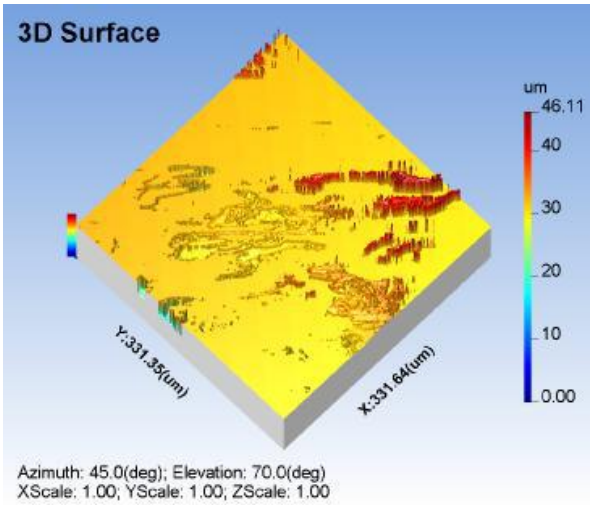


(b) Hexagon pattern.

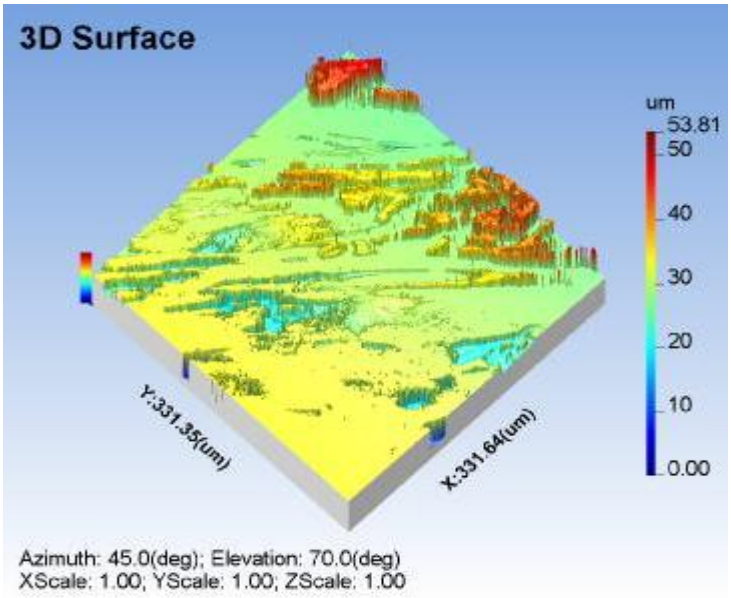


(c) Triangular pattern.

**Fig. 17.** Surface roughness of ILSS fractured surfaces of various patterned 3D-printed composite samples.

## 4. Conclusions

In this work, the effects of FFF process parameters (layer patterns, layer thicknesses and infill densities) on mechanical properties of 3D-printed CF/PLA composite samples have been systematically studied, by conducting tensile, flexural and ILSS tests. The influences of surface roughness on these properties were elucidated and confirmed, using SEM. Therefore, the following conclusions can be drawn based on the results obtained from this innovative study:

- Mechanical properties were greatly influenced by the infill density, pattern and layer thickness (process/slicing parameters). Therefore, these parameters played a major role towards improving the performance of PLA material reinforced with carbon fiber.

- SEM images depicted that the lower infill percent can be attributed to the formation of voids, while the low layer thickness was the main reason for the occurrence of poor bonding at the layer interface as well as between the matrix and the reinforcement.

- Surface roughness played significant role in determining the mechanical properties of the 3D-printed CF/PLA composite samples, as a higher surface roughness value exhibited a decrease in the mechanical properties of the composites.

- Finally, surface roughness significantly depended on the layer height and infill percent. Hence, an extensive study is required to reduce the surface roughness of the AM parts, which consequently contributes to the mechanical strengths of the fabricated structures.

## References


[1] S.A.M. Tofial, E.P. Koumolous, A. Bandyopadhyay, S. Bose, L. O'Donoghue, C. Charitidis, Additive manufacturing: Scientific and technological challenges, market uptake and opportunities, Mater. Today 21 (1) (2018) 22-37.

[2] ASTM F2792-12a, Standard Terminology for Additive Manufacturing Technologies, ASTM International: West Conshohocken, PA (2015).

[3] W. Gao, Y. Zhang, D. Ramanujan, K. Ramani, Y. Chen, C.B. Williams, C.C.L. Wang, Y.C. Shin, S. Zhang, P.D. Zavattieri, The status, challenges, and future of additive manufacturing in engineering, Comput. Aided Des. 69 (2019) 65-89.

[4] Y. Wang, Y. Weng, L. Wang, Characterization of interfacial compatibility of poly lactic acid and bamboo flour (PLA/BF) in biocomposites, Polym. Test. 36 (2014) 119-125.

[5] V.G. Gokhare, D.N. Raut, D.K. Shinde, A review paper on 3D-printing aspects and various processes used in the 3D-printing, Int. J. Eng. Res. Technol. 6 (2017) 953-958.

[6] S. Fafenrot, N. Grimmelsmann, M. Wortmann, A. Ehrmann, Three-dimensional (3D) printing of polymer-metal hybrid materials by fused deposition modeling, Materials 10 (10) (2017) 1199.

[7] C. Comotti, D. Regazzoni, C. Rizzi, A. Vitali, Additive manufacturing to advance functional design: An application in the medical field, J. Comput. Inf. Sci. Eng. 17 (3) (2017) 031006.

[8] Y.Z. Yu, J.R. Lu, J. Liu, 3D printing for functional electronics by injection and package of liquid metals into channels of mechanical structures, Mater. Des. 122 (2017) 80–89.

[9] S.A. Tronvoll, T. Welo, C.W. Elverum, The effects of voids on structural properties of fused deposition modelled parts: A probabilistic approach, Int. J. Adv. Manuf. Technol. 97 (2018) 3607–3618.

[10] J.M. Chacon, M.A. Caminero, E. Garcıa-Plaza, P.J. Nunez, Additive manufacturing of PLA structures using fused deposition modeling: Effect of process parameters on mechanical properties and their optimal selection, Mater. Des. 124 (2017) 143-157.

[11] G. Cicala, D. Giordano, C. Tosto, G. Filippone, A. Recca, I. Blanco, Polylactide (PLA) filaments a biobased solution for additive manufacturing: Correlating rheology and thermomechanical properties with printing quality, Materials 11 (2018) 1191-1204.

[12] L. Yang, S. Li, Y. Li, M. Yang, Q. Yuan, Experimental investigations for optimizing the extrusion parameters on fdm pla printed parts, J. Mater. Eng. Perform. 28 (2019) 169-182.

[13] Y. Magdum, D. Pandey, A.B.S. Harshe, V. Parab, M.S. Kadam, Process parameter optimization for FDM 3D printer, Int. Res J. Eng. Technol. 6 (4) (2019) 1-6.

[14] B. Vikas, M.M. Hussain, C.S. Reddy, Optimization of 3D printing process parameters of poly lactic acid materials by fused deposition modeling process, Int. J. Eng. Dev. Res. 7 (3) (2019) 2321-9939.

[15] J.C. Camargo, A.R. Machado, E.C. Almeida, E.F.M.S. Silva, Mechanical properties of PLA-graphene filament for FDM 3D printing, Int. J. Adv. Manuf. Technol. 103 (2019) 2423-2443.

[16] H.L. Tekinalp, V. Kunc, G.M. Velez-Garcia, C.E. Duty, L.J. Love, A.K. Naskar, C.A. Blue, S. Ozcan, Highly oriented carbon fiber–polymer composites via additive manufacturing, Compos. Sci. Technol. 105 (2014) 144–150.

[17] F. Ning, W. Cong, J. Qiu, J. Wei, S. Wang. Additive manufacturing of carbon fiber reinforced thermoplastic composites using fused deposition modeling, Compos. Part B Eng. 80 (2015) 369-378.

[18] R. Matsuzaki, M. Ueda, M. Namiki, T-K Jeong, H. Asahara, K. Horiguchi, T. Nakamura, A. Todoroki, Y. Hirano, Three-dimensional printing of continuous-fiber composites by in-nozzle impregnation, Sci. Rep. 6 (2016) 1-7.

[19] J. Fernandes, A.M. Deus, L. Reis, M.F. Vaz, M. Leite, Study of the influence of 3printing parameters on the mechanical properties of PLA, In Proceedings of the 3rd International Conference on Progress in Additive Manufacturing, Singapore, (2018) 14–17.

[20] M.A. Caminero, J.M. Chacon, E. Garcia-Plaza, P.J. Nunez, J.M. Reverte, J.P. Becar, Additive manufacturing of PLA-based composites using fused filament fabrication: Effect of graphene nano platelet reinforcement on mechanical properties, dimensional accuracy and texture, Polymers 11 (2019) 799.

[21] K. Vigneshwaran, N. Venkateshwaran, Statistical analysis mechanical properties of wood–PLA prepared via additive manufacturing, Int. J. Polym. Analy. Charact. 24 (2019) 584-596.

[22] M.A. Quanjin, I.M. Sahat, M.R.M. Rejab, S.A. Hassan, B. Zhang, M.N.M. Merzuki, The energy absorbing characteristics of filament wound hybrid carbon fiber reinforced plastic/polylactic acid tubes with different infill pattern structures, J. Reinf. Plas. Compos. 38 (2019) 1067-1088.

[23] M.N. Sudin, S.A. Shamsudin, M.A. Abdullah, Effect of part features on dimensional accuracy of FDM model, J. Eng. Appl. Sci. 11 (13) (2016) 8067–8072.

[24] N.S.A. Bakar, M.R. Alkahari, H. Boejang, Analysis on fused deposition modeling performance, J. Zhejiang Univ. Sci. A 11 (2010) 972–977.

[25] G. Dyrbuś, Investigation on quality of rapid prototyping FDM method, 14th International Research. In Expert Conference, Trends in the Development of Machinery and Associated Technology, (2010) Mediterranean Cruise.TMT (2010), 11-18.

[26] L.M. Galantucci, I. Bodi, J. Kacani, Analysis of dimensional performance for a 3D open-source printer based on fused deposition modeling technique, Proced. CIRP 28 (2015) 82-87.

[27] H.A. Habeeb, F.R. Ramli, R. Hasan**,** Strength and porosity of additively manufactured PLA using a low cost 3D printing, Conference: Mechanical Engineering Research Day 2016: Malaysia.

[28] G. Strano, L. Hao, R.M. Everson, K.E. Evans, Surface roughness analysis, modeling and prediction in selective laser melting, J. Mater. Process. Technol. 213 (2013) 589–597.

[29] P.M. Pandey, V. Reddy, S.G. Dhande, Slicing procedures in layered manufacturing: A review, Rapid Prototyp. J. 9 (2003) 274–288.

[30] M. Altan, M. Eryildiz, B. Gumus, Y. Kahraman, Effects of process parameters on the quality of PLA products fabricated by fused deposition modeling (FDM): Surface roughness and tensile strength, Mater. Test. 60 (2018) 471–477.

[31] M. Pérez, G. Medina-Sánchez, A. García-Collado, M. Gupta, D. Carou, Surface quality enhancement of fused deposition modeling (FDM) printed samples based on the selection of critical printing parameters, Materials 11 (2018) 1382-1395.

[32] I. Buj-Corral, A. Domínguez-Fernández, R. Durán-Llucià, Influence of print orientation on surface roughness in fused deposition modeling (FDM) processes, Materials 12 (2019) 3834-3849.

[33] J.A. Taborda-Rios, O. Lopez-Botello, P. Zambrano-Robledo, L.A. Reyes-Osorio, C. Garza, Mechanical characterisation of a bamboo fibre/poly lactic acid composite produced by fused deposition modeling, J. Reinf. Plast. Compos. 39 (23–24) (2020) 932–944.

[34] A.N. Dickson, J.N. Barry, K.A. McDonnell, D.P. Dowling, Fabrication of continuous carbon, glass and kevlar fibre reinforced polymer composites using additive manufacturing, Addit. Manuf. 16 (2017) 146–152.

[35] V. Mazzanti, L. Malagutti, F. Mollica, FDM 3D printing of polymers containing natural fillers: A review of their mechanical properties, Polymers 11 (7) (2019) 1094.

[36] D. Depuydt, M. Balthazar, K. Hendrickx, W. Six, E. Ferraris, F. Desplentere, J. Ivens, A.W.V. Vuure, Production and characterization of bamboo and flax fiber reinforced polylactic acid filaments for fused deposition modeling (FDM), Polym. Compos. 40 (2019) 1951–1963.